Re-submitted to the International Journal for Numerical Methods in Engineering in December 2014

The X-FEM with new crack-tip enrichment functions for an interface crack between two dissimilar piezoelectric materials

P. Ma[1], R. K. L. Su[1,*], W. J. Feng[2,*], Y. S. Li[3]

[1] *Department of Civil Engineering, The University of Hong Kong, PR China*

[2] *Department of Engineering Mechanics, Shijiazhuang Tiedao University, Shijiazhuang 050043, PR China*

[3] *College of Civil Engineering, Hebei University of Engineering, Handan 056038, PR China*

SUMMARY

This paper studies the static fracture problems of an interface crack in linear piezoelectric bimaterial by means of the extended finite element method (X-FEM) with new crack-tip enrichment functions. In the X-FEM, crack modelling is facilitated by adding a discontinuous function and the crack-tip asymptotic functions to the classical finite element approximation within the framework of the partition of unity. In this work the coupled effects of an elastic field and an electric field in piezoelectricity is considered. Corresponding to two classes of singularities of the aforementioned interface crack problem, namely ε class and κ class, two classes of crack-tip enrichment functions are newly derived and the former which exhibits oscillating feature at the crack tip is numerically investigated. Computation of the fracture parameter, i.e. the *J*-integral, using the domain form of the contour integral, is presented. Excellent accuracy of the proposed formulation is demonstrated on benchmark interface crack problems through comparisons with analytical solutions and numerical results obtained by the classical finite element method (FEM). Moreover, it is shown that the geometrical enrichment combining the mesh with local refinement is substantially better in terms of accuracy and efficiency.

KEY WORDS: extended finite element method; piezoelectric materials; interface crack; *J*-integral; oscillating singularity

[*] Corresponding author. Tel: +852 2859 2648; fax: +852 2559 5337
E-mail address: klsu@hku.hk (R.K.L. Su); wjfeng9999@126.com (W.J. Feng).

1. INTRODUCTION

As a powerful tool in computation fracture mechanics, the extended finite element method (X-FEM) was originally proposed by Belytschko and Black [1]. In the X-FEM, crack discontinuity is represented by enriching the classical finite element approximation by discontinuous and crack-tip enrichment functions based on the framework of the partition of unity. A state-of-the-art review of the X-FEM for computational fracture mechanics can be found in [2-5]. Recently, the X-FEM has been successfully applied to solve the crack problem of piezoelectric materials [6-12]. Among them, Béchet et al. [6] firstly applied the X-FEM to the fracture of piezoelectric materials and derived new crack-tip enrichment functions. Bhargava and Sharma [7, 8] further studied the size effect and two-unequal-collinear crack problem in piezoelectric materials by means of the X-FEM. Sharma et al. [9] analyzed a subinterface crack in piezoelectric bimaterial with the X-FEM. Liu et al. [10, 11] studied the crack problems for functionally graded piezoelectric materials under electromechanical and thermal impacts, respectively. Nguyen-Vinh et al. [12] investigated the dynamic fracture of piezoelectric materials employing the X-FEM. Bui and Zhang [13] applied the X-FEM to simulate the stationary dynamic cracks in piezoelectric bodies under impact loading. Nanthakumar et al. [14, 15] proposed an effective iteration method to solve the inverse problem of detecting voids and cracks in piezoelectric structures using the X-FEM. Alternatively, a number of numerical techniques are also turned out to be very efficient to solve complex fracture problems, such as the special crack-tip elements [16], the embedded finite element method [17-23], the cracking particles method [24-28] and the phase-field models [29, 30]. Most of these numerical methods have been extended to the crack analysis in piezoelectric materials [31-41].

On the other hand, considerable analytical studies have been conducted to investigate the two-dimentional (2-D) interface crack problem in a piezoelectric bimaterial [42-60]. However, owing to the mathematical complexity, all these theoretical studies are limited to the interface cracks between two semi-infinite planes or two infinite strips. Also, until now, several numerical methods have

been proposed to solve the interface crack problem in piezoelectric bimaterial. For example, Liew and Liang [61] presented a numerical model for three-dimensional (3-D) piezoelectric bimaterials based on the boundary element method (BEM). Guo and Fang [62] studied the fracture behaviors of interface cracks in piezoelectric bimaterials employing the developed element free Galerkin method (EFG). In connection with the classical finite element method (FEM), Govorukha and Kamlah [63, 64] derived the asymptotic solutions to the interface crack problem. Scherzer and Kuna [65] proposed a new technique to bypass possible singular oscillatory terms by means of orthogonalized eigenfunctions. Benedetti et al. [66] presented a fast boundary element method for the analysis of 3-D solids with cracks and bonded piezoelectric patches. Sladek et al. [67, 68] put forward a meshless method based on the local Petrov-Galerkin approach and applied it to analyse the electrically impermeable and permeable interface crack problem. Lei and Zhang [69] and Lei et al. [70] studied the transient response of interfacial cracks under electromechanical impacts by a time-domain boundary element method. Li et al. [71] extended the scaled boundary finite element method (SBFEM) to investigate the dynamic field intensity factors of electrically impermeable interface cracks. However, to our best knowledge, application of the X-FEM to fracture analysis on the interface crack problem in a piezoelectric bimaterial has not been reported yet; in particular, the suitable crack-tip enrichment functions for the aforementioned problem are still not available to date.

Therefore, in this paper, corresponding to two classes of singularities of interface cracks between two dissimilar transversely isotropic piezoelectric materials, namely ε class and κ class, we newly derive two classes of crack-tip enrichment functions and present the X-FEM analysis on the former, which can be regarded as a new topic owing to its oscillating behaviour near the crack tip. Following the introduction, the basic equations are briefly given in Section 2, and the basic extended finite element formulation is clearly provided in Section 3. The crack-tip asymptotic fields of generalised displacement and new crack-tip enrichment functions suitable for an interface crack

in a piezoelectric bimaterial are presented in Section 4. The computation of fracture parameters using the domain form of the contour integral is described in Section 5 and supportive numerical results and discussions are presented in Section 6 to verify the formulation. The last section presents the main findings drawn from the theoretical and numerical results.

2. BASIC EQUATIONS FOR PIEZOELECTRIC SOLIDS

2.1. Field equations

In the rectangular Cartesian coordinate system x_i $(i=1,2,3)$, the governing equations for piezoelectric materials may be written in the following form

$$\begin{cases} \sigma_{ij} = c_{ijks}\varepsilon_{ks} - e_{sij}E_s \\ D_i = e_{iks}\varepsilon_{ks} + \alpha_{is}E_s \end{cases} \tag{1}$$

$$\varepsilon_{ij} = \frac{1}{2}\left(u_{i,j} + u_{j,i}\right), \quad E_i = -\varphi_{,i} \tag{2}$$

$$\sigma_{ij,j} = -f_i^{mech}, \quad D_{i,i} = f^e \tag{3}$$

where σ_{ij} and D_i are the components of the stresses and electrical displacements, respectively; ε_{ij} and E_i are the components of strains and electrical fields, respectively; and u_i and φ are the mechanical displacement components and electrical potential, respectively. c_{ijks}, e_{iks} and α_{is} are the elastic, piezoelectric constants and dielectric permittivities, respectively. f_i^{mech} and f^e are the body force and electric charge density, respectively. i, j, k, s range in $\{1,2,3\}$, the repeated indexes imply summation and the comma stands for the differentiation with respect to the corresponding coordinate variables.

In this paper, we consider transversely isotropic piezoelectric materials poled in the direction x_3 under plane strain conditions, which have an essential practical significance. In this situation, the constitutive equations can be further reduced to

$$\begin{Bmatrix}\sigma_{11}\\ \sigma_{33}\\ \sigma_{13}\\ D_1\\ D_3\end{Bmatrix}=\begin{bmatrix}c_{11} & c_{13} & 0 & 0 & -e_{31}\\ c_{13} & c_{33} & 0 & 0 & -e_{33}\\ 0 & 0 & c_{44} & -e_{15} & 0\\ 0 & 0 & e_{15} & \alpha_{11} & 0\\ e_{31} & e_{33} & 0 & 0 & \alpha_{33}\end{bmatrix}\begin{Bmatrix}\varepsilon_{11}\\ \varepsilon_{33}\\ 2\varepsilon_{13}\\ E_1\\ E_3\end{Bmatrix} \tag{4}$$

2.2. Boundary conditions

As shown in Figure 1, a piezoelectric bimaterial system consists of two dissimilar materials which occupy the domains Ω_1 and Ω_2, respectively. The problem domain $\Omega=\Omega_1\bigcup\Omega_2$, and its outer boundary are denoted by Γ. A crack $\Gamma_c=\Gamma_c^+\bigcup\Gamma_c^-$ is situated at the interface of the two materials. Γ is subjected to the following boundary conditions: electromechanical load is imposed on Γ_t (natural boundary conditions), whereas the extended displacements, namely displacement and electrical potential, are prescribed on Γ_u (essential boundary conditions). The crack faces Γ_c^+ and Γ_c^- are assumed to be traction-free and electrically impermeable herein. The boundary conditions are summarized as

$$\begin{cases}\sigma_{ij}n_j=0\\ D_in_i=0\end{cases}\quad \text{on}\quad \Gamma_c^+\bigcup\Gamma_c^- \tag{5a}$$

$$\begin{cases}\sigma_{ij}n_j=t_i^0\\ D_in_i=D^0\end{cases}\quad \text{on}\quad \Gamma_t \tag{5b}$$

$$\begin{cases}u_j=u_j^0\\ \varphi=\varphi^0\end{cases}\quad \text{on}\quad \Gamma_u \tag{5c}$$

3. EXTENDED FINITE ELEMENT FORMULATION

The classical FEM has been widely applied to crack problems in piezoelectric materials, and a detailed survey was given by Kuna [72, 73]. The classical FEM requires that the boundary of element mesh conforms to the crack faces and therefore double nodes are prescribed on the crack

faces. However, the modelling of cracks using the X-FEM is independent of element shape or meshing, which simplifies the mesh generation and avoids remeshing as the crack propagates. The interface cracks in a bimaterial can also be modelled by changing the nodal properties on crack faces without using double nodes in the X-FEM. Moreover, in the classical FEM, the special crack-tip elements (CTE), for example, the quarter-point elements, are commonly employed to account for the stress field singularity with a strength of $1/\sqrt{r}$, and have been proved to produce accurate results for piezoelectric solids [31-34]. However, this sort of elements is only applicable to model the real singularity near crack tip, e.g., inverse square root singularity. For the complex singularity of interface crack problems in a bimaterial, those elements cannot capture the oscillating feature of the displacements and the stresses in the vicinity of a crack tip. The X-FEM, however, can satisfactorily address this problem by means of the suitable crack-tip enrichment functions.

The extended finite element approximation for the displacement and electrical potential for impermeable boundary conditions is written as [4-6, 9]

$$\mathbf{u}^h(\mathbf{x}) = \sum_{i\in N} N_i(\mathbf{x})\mathbf{u}_i + \sum_{j\in N^H} N_j(\mathbf{x})\left[H\left(f(\mathbf{x})\right) - H\left(f(\mathbf{x}_j)\right)\right]\boldsymbol{a}_j + \sum_{k\in N^{CT}} N_k(\mathbf{x})\sum_{\alpha}\left[F_\alpha(\mathbf{x}) - F_\alpha(\mathbf{x}_k)\right]\boldsymbol{b}_k^\alpha \quad (6)$$

where N_i is the standard finite element shape function related to node *i*; $\mathbf{u}_i$ is a 3-component vector of nodal degree of freedom since three nodal variables (u_1, u_3, ϕ) are involved; F_α is the α th component of crack-tip enrichment functions; $\boldsymbol{a}_j$ and $\boldsymbol{b}_k^\alpha$ are, respectively, the nodal degree of freedom vector associated with the functions H and F_α; $f(\mathbf{x})$ denotes an implicit function description (i.e., a level set) and $H(t)$ is the generalised Heaviside function

$$H(t) = \begin{cases} 1, & t > 0 \\ -1, & t \le 0 \end{cases} \quad (7)$$

Figure 2 shows the enrichment scheme, in which the nodes enriched by the Heaviside function (set N^H) are marked with open circles whereas the nodes enriched by crack-tip enrichment functions (set N^{CT}) are marked with filled circles. Two kinds of enrichment strategies, namely

topological enrichment and geometrical (fixed area) enrichment, are presented in Figure 2. The former only enriches the nodes directly related to the crack tip (Figure 2a) and the latter spans all nodes lying inside a circle of radius r_e centred at the crack tip (Figure 2b), which is useful to improve the X-FEM accuracy [6, 74]. It is remarked that crack-tip enrichment will be used if one node is simultaneously enriched by the aforementioned two kinds of functions.

After the approximate discretization of the governing equations, the standard discrete system of equations is obtained as

$$\mathbf{K}\mathbf{u}^h = \mathbf{f} \tag{8}$$

where $\mathbf{K}$ is the stiffness matrix and $\mathbf{f}$ is the external force vector. The system matrix and vectors are developed by assembling the matrix and vectors of each element. $\mathbf{K}$ and $\mathbf{f}$ for each element are defined as

$$\mathbf{k}_{ij}^e = \begin{bmatrix} \mathbf{k}_{ij}^{uu} & \mathbf{k}_{ij}^{ua} & \mathbf{k}_{ij}^{ub} \\ \mathbf{k}_{ij}^{au} & \mathbf{k}_{ij}^{aa} & \mathbf{k}_{ij}^{ab} \\ \mathbf{k}_{ij}^{bu} & \mathbf{k}_{ij}^{ba} & \mathbf{k}_{ij}^{bb} \end{bmatrix} \tag{9a}$$

$$\mathbf{f}_i^e = \left\{ \mathbf{f}_i^u \quad \mathbf{f}_i^a \quad \mathbf{f}_i^{b1} \quad \mathbf{f}_i^{b2} \quad \cdots\cdots \quad \mathbf{f}_i^{bl} \right\}^{\mathrm{T}} \tag{9b}$$

where *u*, *a* and *b* refer to the extended displacement vectors and the extended new (enriched) degree of freedom vectors and l is the number of the components of crack-tip enrichment functions, so that

$$\mathbf{k}_{ij}^{rs} = \int_{\Omega_e} \left(\mathbf{B}_i^r \right)^{\mathrm{T}} \mathbf{C} \left(\mathbf{B}_j^s \right) \mathrm{d}\Omega, \quad (r, s = u, a, b) \tag{10a}$$

$$\mathbf{f}_i^u = \int_{\partial\Omega_e} N_i \overline{\mathbf{t}} \mathrm{d}\Gamma + \int_{\Omega_e} N_i \overline{\mathbf{f}} \mathrm{d}\Omega, \quad \mathbf{f}_i^a = \int_{\partial\Omega_e} \hat{S}_i \overline{\mathbf{t}} \mathrm{d}\Gamma + \int_{\Omega_e} \hat{S}_i \overline{\mathbf{f}} \mathrm{d}\Omega \tag{10b}$$

$$\mathbf{f}_i^{b\alpha} = \int_{\partial\Omega_e} S_i^{\alpha} \overline{\mathbf{t}} \mathrm{d}\Gamma + \int_{\Omega_e} S_i^{\alpha} \overline{\mathbf{f}} \mathrm{d}\Omega, \quad (\alpha = 1, 2, \cdots\cdots, l) \tag{10c}$$

where $\overline{\mathbf{t}}$ and $\overline{\mathbf{f}}$ are the prescribed extended tractions and volume force vector, respectively, and

$$\hat{S}_i = N_i \left[H\left(f\left(\mathbf{x}\right)\right) - H\left(f\left(\mathbf{x}_i\right)\right) \right] \tag{11a}$$

$$S_i^\alpha = \begin{cases} \tilde{S}_i^\alpha = N_i\left[\tilde{F}_\alpha(\mathbf{x}) - \tilde{F}_\alpha(\mathbf{x}_i)\right], & \text{for elastic field,} \\ \hat{S}_i^\alpha = N_i\left[\hat{F}_\alpha(\mathbf{x}) - \hat{F}_\alpha(\mathbf{x}_i)\right], & \text{for electric field,} \end{cases} \qquad F_\alpha = \begin{cases} \tilde{F}_\alpha, & \text{for elastic field,} \\ \hat{F}_\alpha, & \text{for electric field,} \end{cases} \tag{11b}$$

$\tilde{F}_\alpha$ and $\hat{F}_\alpha$ are, respectively, the α th component of crack-tip enrichment functions for elastic field $\tilde{\mathbf{F}}$ and electric field $\hat{\mathbf{F}}$. They are extracted from the analytical solution, and will be provided in the next section. In Equation (10a), $\mathbf{B}_i^u$, $\mathbf{B}_i^a$ and $\mathbf{B}_i^b$ are the matrices of shape function derivatives, and

$$\mathbf{B}_i^u = \begin{bmatrix} N_{i,x} & 0 & 0 \\ 0 & N_{i,y} & 0 \\ N_{i,y} & N_{i,x} & 0 \\ 0 & 0 & N_{i,x} \\ 0 & 0 & N_{i,y} \end{bmatrix}, \quad \mathbf{B}_i^a = \begin{bmatrix} \hat{S}_{i,x} & 0 & 0 \\ 0 & \hat{S}_{i,y} & 0 \\ \hat{S}_{i,y} & \hat{S}_{i,x} & 0 \\ 0 & 0 & \hat{S}_{i,x} \\ 0 & 0 & \hat{S}_{i,y} \end{bmatrix} \tag{12a}$$

$$\mathbf{B}_i^b = \begin{bmatrix} \mathbf{B}_i^{b1} & \mathbf{B}_i^{b2} & \cdots\cdots & \mathbf{B}_i^{bl} \end{bmatrix} \tag{12b}$$

$$\mathbf{B}_i^{b\alpha} = \begin{bmatrix} \tilde{S}_{i,x}^\alpha & 0 & 0 \\ 0 & \tilde{S}_{i,y}^\alpha & 0 \\ \tilde{S}_{i,y}^\alpha & \tilde{S}_{i,x}^\alpha & 0 \\ 0 & 0 & \hat{S}_{i,x}^\alpha \\ 0 & 0 & \hat{S}_{i,y}^\alpha \end{bmatrix} \tag{12c}$$

4. GENERALISED DISPLACEMENT FIELDS AND NEW ENRICHMENT FUNCTIONS FOR AN INTERFACE CRACK IN A PIEZOELECTRIC BIMATERIAL

For the crack problem in isotropic elastic materials, the crack-tip enrichment functions are

$$\mathbf{F}(r,\theta) = \sqrt{r}\left[\sin\frac{\theta}{2},\ \cos\frac{\theta}{2},\ \sin\frac{\theta}{2}\sin\theta,\ \cos\frac{\theta}{2}\sin\theta\right] \tag{13}$$

These functions are also called standard four-fold enrichment functions or isotropic enrichment functions. As the simplest enrichment functions, they have been used to model the near-tip displacement field in homogeneous piezoelectric materials [6-8]. In the present study, we will derive new crack-tip enrichment functions for an interface crack in a piezoelectric bimaterial.

Since we are mainly interested in the singularity at the crack tip, a semi-infinite crack model is employed, which is simpler to obtain analytical solutions. Referring to [42, 43, 64], the general solution for a two-dimensional problem can be expressed as

$$\mathbf{u}^{(m)} = \left[u_1^{(m)}, u_3^{(m)}, \varphi^{(m)} \right]^{\mathrm{T}} = \mathbf{A}^{(m)} \mathbf{f}^{(m)}\left(z\right) + \overline{\mathbf{A}^{(m)} \mathbf{f}^{(m)}\left(z\right)} \tag{14}$$

$$\mathbf{t}^{(m)} = \left[\sigma_{31}^{(m)}, \sigma_{33}^{(m)}, D_3^{(m)} \right]^{\mathrm{T}} = \mathbf{B}^{(m)} \mathbf{f}'^{(m)}\left(z\right) + \overline{\mathbf{B}^{(m)} \mathbf{f}'^{(m)}\left(z\right)} \tag{15}$$

where subscript m=1, 2 stands for the upper and the lower materials, respectively; $z_s = x_1 + p_s x_3 \left(s = 1, 2, 3\right)$, $\mathbf{f}$ is an arbitrary vector function to be determined; and p_s and $\mathbf{a}_s$ are the eigenvalues with positive imaginary parts and eigenvectors, respectively, obtained from the equation $[\mathbf{Q} + p\left(\mathbf{R} + \mathbf{R}^{\mathrm{T}}\right) + p^2\mathbf{T}]\mathbf{a} = 0$, where $\mathbf{Q}$, $\mathbf{R}$ and $\mathbf{T}$ are defined in Stroh's formalism as $\mathbf{Q}_{JK} = C_{1JK1}$, $\mathbf{R}_{JK} = C_{1JK3}$ and $\mathbf{T}_{JK} = C_{3JK3}$. $\mathbf{A}$ is a matrix composed of $\mathbf{a}_s$, and $\mathbf{B} = \mathbf{R}^{\mathrm{T}}\mathbf{A} + \mathbf{TAP}$ [43, 57], where $\mathbf{P} = \mathrm{diag}\left[p_1,\ p_2,\ p_3 \right]$.

For an electrically impermeable crack, the continuity and boundary conditions at the interface can be written as

$$\mathbf{u}^{(1)}\left(x_1, 0\right) = \mathbf{u}^{(2)}\left(x_1, 0\right), \quad \mathbf{t}^{(1)}\left(x_1, 0\right) = \mathbf{t}^{(2)}\left(x_1, 0\right), \quad x_1 \notin \Gamma_c \tag{16a}$$

$$\mathbf{t}^{(1)}\left(x_1, 0\right) = \mathbf{t}^{(2)}\left(x_1, 0\right) = 0, \quad x_1 \in \Gamma_c \tag{16b}$$

Assuming $\mathbf{f}^{(m)} = \left\langle \left(z_s^{(m)} \right)^{\delta} \right\rangle \mathbf{q}^{(m)}$, where $\langle\ \rangle$ indicates the diagonal matrix with each component varying according to s, and using $z_s = r\left(\cos\theta + p_s \sin\theta\right)$ in polar coordinates, Equations (14) and (15) can be rewritten as [75]

$$\mathbf{u}^{(m)} = r^{\delta} \left[\mathbf{A}^{(m)} \left\langle \left(\cos\theta + p_s^{(m)} \sin\theta \right)^{\delta} \right\rangle \mathbf{q}^{(m)} + \overline{\mathbf{A}}^{(m)} \left\langle \left(\cos\theta + \overline{p}_s^{(m)} \sin\theta \right)^{\delta} \right\rangle \overline{\mathbf{q}}^{(m)} \right] \tag{17}$$

$$\mathbf{t}^{(m)} = \delta r^{\delta-1} \left[\mathbf{B}^{(m)} \left\langle \left(\cos\theta + p_s^{(m)} \sin\theta \right)^{\delta-1} \right\rangle \mathbf{q}^{(m)} + \overline{\mathbf{B}}^{(m)} \left\langle \left(\cos\theta + \overline{p}_s^{(m)} \sin\theta \right)^{\delta-1} \right\rangle \overline{\mathbf{q}}^{(m)} \right] \tag{18}$$

For $\theta = \pm\pi$ and $\theta = 0$, we have

$$z_s = \begin{cases} r\mathrm{e}^{\pm \mathrm{i}\pi}, & \theta = \pm\pi \\ r, & \theta = 0 \end{cases} \tag{19}$$

Substituting Equations (17) and (18) into Equation (16) and introducing matrix $\mathbf{Y} = \mathrm{i}\mathbf{A}\mathbf{B}^{-1}$, one gets [75]

$$\left[\mathbf{H} + e^{2\pi\mathrm{i}(\delta-1)}\overline{\mathbf{H}}\right]\mathbf{B}^{(1)}\mathbf{q}^{(1)} = 0 \tag{20}$$

where $\mathbf{H} = \mathbf{Y}^{(1)} + \overline{\mathbf{Y}}^{(2)} = \mathbf{D} + \mathrm{i}\mathbf{W}$. Ou and Wu [48] have shown that for the transversely isotropic piezoelectric materials considered in the present study, $c = \left|\mathbf{D}^{-1}\mathbf{W}\right| = 0$ holds true and the singularity of the present problem defined by the roots of Equation (20) can be classified into two classes: (1) if b<0, $\delta_{1,2} = 1/2 \pm \mathrm{i}\varepsilon$, $\delta_3 = 1/2$; (2) if b>0, $\delta_{1,2} = 1/2 \pm \kappa$, $\delta_3 = 1/2$, where ε and κ are real, and

$$\varepsilon = \frac{1}{\pi}\tanh^{-1}\sqrt{-2b}\,,\ \kappa = \frac{1}{\pi}\tan^{-1}\sqrt{2b} \tag{21}$$

$$b = \frac{1}{4}\left[\mathrm{tr}\left(\mathbf{D}^{-1}\mathbf{W}\right)^2\right] \tag{22}$$

The former is called ε-class (oscillating singularity), and the latter is called κ-class (non-oscillating singularity) [48]. The crack-tip enrichment functions for the two cases will be derived separately.

(i) ε-class (oscillating singularity)

For the present plane strain problem, there are six eigenvalues for each piezoelectric material, namely $p_1^{(m)}$, $p_2^{(m)}$ and $p_3^{(m)}$, with positive imaginary parts and their conjugates complex $p_4^{(m)} = \overline{p}_1^{(m)}$, $p_5^{(m)} = \overline{p}_2^{(m)}$, $p_6^{(m)} = \overline{p}_3^{(m)}$. For the ε-class problem, the stresses near the crack tip have the oscillating singularity while electric displacement has inverse square root singularity according to Equation (18). The difference in the singularities above leads to different crack-tip enrichment functions and, therefore, the crack-tip enrichment functions for the elastic field and electric field should be derived, respectively.

First, we consider the elastic field, which corresponds to $\delta_{1,2}=1/2\pm \mathrm{i}\varepsilon$; as the necessary part for deriving the enrichment functions, the term $r^{\delta}\left[\cos\theta+p_t^{(m)}\sin\theta\right]^{\delta}\quad (t=1,2,\cdots,6)$ in Equation (17) for each arbitrary eigenvalue $p_t^{(m)}$ can be expressed as

$$\sqrt{r}\sqrt{\beta_t^{(m)}}e^{-\varepsilon\psi_t^{(m)}}\left[\cos\left(\varepsilon\ln r\right)+\mathrm{i}\sin\left(\varepsilon\ln r\right)\right]\left[\cos\left(\vartheta_t^{(m)}\right)+\mathrm{i}\sin\left(\vartheta_t^{(m)}\right)\right] \tag{23}$$

where

$$\vartheta_t^{(m)}=\varepsilon\ln\beta_t^{(m)}+\frac{\psi_t^{(m)}}{2} \tag{24a}$$

$$\beta_t^{(m)}=\sqrt{\left[\cos\theta+\mathrm{Re}\left(p_t^{(m)}\right)\sin\theta\right]^2+\left[\mathrm{Im}\left(p_t^{(m)}\right)\sin\theta\right]^2} \tag{24b}$$

$$\psi_t^{(m)}=\arg\left[\cos\theta+\mathrm{Re}\left(p_t^{(m)}\right)\sin\theta+\mathrm{i}\,\mathrm{Im}\left(p_t^{(m)}\right)\sin\theta\right] \tag{24c}$$

$\mathrm{Re}(z)$ and $\mathrm{Im}(z)$ are the real part and imaginary part of complex z; arg(z) denotes the principal argument of complex z. The crack-tip enrichment functions for the elastic field for an arbitrary eigenvalue $p_t^{(m)}$ can be extracted from (23) and are presented as

$$\tilde{\mathbf{F}}_t^{(m)}(r,\theta)=\sqrt{r}\sqrt{\beta_t^{(m)}}e^{-\varepsilon\psi_t^{(m)}}\left[\tilde{F}_{t1}^{(m)}(r,\theta),\ \tilde{F}_{t2}^{(m)}(r,\theta),\ \tilde{F}_{t3}^{(m)}(r,\theta),\ \tilde{F}_{t4}^{(m)}(r,\theta)\right],\ t=1,2,\cdots,6 \tag{25}$$

$$\tilde{F}_{t1}^{(m)}(r,\theta)=\cos\left(\varepsilon\ln r\right)\cos\left(\vartheta_t^{(m)}\right),\quad \tilde{F}_{t2}^{(m)}(r,\theta)=\cos\left(\varepsilon\ln r\right)\sin\left(\vartheta_t^{(m)}\right) \tag{26a}$$

$$\tilde{F}_{t3}^{(m)}(r,\theta)=\sin\left(\varepsilon\ln r\right)\cos\left(\vartheta_t^{(m)}\right),\quad \tilde{F}_{t4}^{(m)}(r,\theta)=\sin\left(\varepsilon\ln r\right)\sin\left(\vartheta_t^{(m)}\right) \tag{26b}$$

By assembling the enrichment functions for each eigenvalue and only retaining the independent components, the whole crack-tip enrichment functions for the elastic field can be presented as

$$\tilde{\mathbf{F}}^{(m)}(r,\theta)=\left[\tilde{\mathbf{F}}_1^{(m)}(r,\theta),\ \tilde{\mathbf{F}}_2^{(m)}(r,\theta),\ \tilde{\mathbf{F}}_3^{(m)}(r,\theta),\ \tilde{\mathbf{F}}_4^{(m)}(r,\theta),\ \tilde{\mathbf{F}}_5^{(m)}(r,\theta),\ \tilde{\mathbf{F}}_6^{(m)}(r,\theta)\right] \tag{27}$$

On the other hand, for the interfacial crack problem the electric displacement exhibits the classical $1/\sqrt{r}$ singularity behavior near the crack tip. This is consistent with the internal crack problem in a homogeneous piezoelectric material, in which both stresses and electrical

displacement have the classical inverse square root singularity. The aforementioned real singularity makes the crack-tip enrichment functions for the electric field rather simple. By setting $\varepsilon = 0$ in Equation (27), the corresponding crack-tip enrichment functions for the electric field concerning $p_t^{(m)}$ can be readily acquired as

$$\widehat{\mathbf{F}}^{(m)}(r,\theta) = \left[\widehat{\mathbf{F}}_1^{(m)}(r,\theta),\ \widehat{\mathbf{F}}_2^{(m)}(r,\theta),\ \widehat{\mathbf{F}}_3^{(m)}(r,\theta)\right] \tag{28}$$

where

$$\widehat{\mathbf{F}}_s^{(m)}(r,\theta) = \left[\widehat{F}_{s1}^{(m)}(r,\theta),\ \widehat{F}_{s2}^{(m)}(r,\theta)\right] = \sqrt{r\beta_s^{(m)}}\left[\cos\left(\frac{\psi_s^{(m)}}{2}\right),\ \sin\left(\frac{\psi_s^{(m)}}{2}\right)\right],\ s = 1,2,3 \tag{29}$$

In this way, we have obtained the crack-tip enrichment functions for the elastic field and electric field, i.e., Equations (27) and (28), respectively. For arbitrary angles of poling direction with respect to the crack path, Béchet et al. [6] developed the crack-tip enrichment functions for cracks in homogeneous piezoelectric materials. If we assume that the poling direction is perpendicular to the crack faces, which is considered in the present paper, the corresponding crack-tip enrichment functions in Béchet et al. [6] and Bhargava and Sharma [8] are consistent with Equation (28). Additionally, if further neglecting the electric field, namely $\widehat{\mathbf{F}}_3(r,\theta)$, the crack-tip enrichment functions composed of $\widehat{\mathbf{F}}_1(r,\theta)$ and $\widehat{\mathbf{F}}_2(r,\theta)$ in Equation (28) agree with those in Asadpoure and Mohammadi [76] for the homogeneous orthotropic elastic materials. Moreover, Equation (27) shows that a total of 24 crack-tip enrichment functions are obtained for the interface crack problem in piezoelectric bimaterial, compared with the case of isotropic elastic bimaterial in which 12 are proposed in Sukumar et al. [77]. This is owing to the special material property of piezoelectric solids. However, in Equation (28) the crack-tip enrichment functions for the electric field only have six components. The reason for this is that the electric field possesses a real singularity, and in this situation $p_t^{(m)}$ and $\overline{p}_t^{(m)}$ will lead to identical enrichment functions, which greatly reduces the number of crack-tip enrichment functions.

It is noted that for the present interface crack problem, the component numbers of the crack-tip enrichment functions for the elastic field and electric field are different according to Equations (27) and (28). As previously mentioned, Equation (28) is a special case of Equation (27) as the oscillating index $\varepsilon = 0$. Hence when assembling the system stiffness matrix, for convenience, we can still regard Equation (28) as a vector with 24 components, in which only six of them, namely, the 1st, 2nd, 5th, 6th, 9th, 10th are effective and the other 18 components are equal to zero. However, these zero components of crack-tip enrichment functions for the electric field will lead to linear dependence or the fact that all the elements of the corresponding rows and columns in the system stiffness matrix equal to zero. Obviously, this will result in the appearance of singularity in the system stiffness matrix. Therefore, in order to avoid the singular solution problem, the added nodal degrees of freedom $\boldsymbol{b}_k^{\alpha}$ associated with the aforementioned zero components of crack-tip enrichment functions for the electric field will be set as zero in the FEM pre-processing, which can be regarded as the generalised essential boundary conditions.

In addition, it is worth mentioning that two pairs of crack-tip enrichment functions, namely $\tilde{\mathbf{F}}^{(1)}$ and $\widehat{\mathbf{F}}^{(1)}$ corresponding to material 1 and $\tilde{\mathbf{F}}^{(2)}$ and $\widehat{\mathbf{F}}^{(2)}$ corresponding to material 2, should be adopted in numerical analysis since different material constants produce different eigenvalues $p_t^{(m)}$. Additionally, the enrichment functions (27) are applicable to the interface crack problem in anisotropic elastic bimaterials if neglecting the components relating to the piezoelectric phase.

(ii) κ-class (non-oscillating singularity)

Considering that all singularities are real for κ-class bimaterial, the enrichment functions are formally similar to Equation (28) in this case. For completeness, they are presented as follows

$$\tilde{\mathbf{F}}^{(m)}(r,\theta) = \left[\tilde{\mathbf{F}}_1^{(m)}(r,\theta),\ \tilde{\mathbf{F}}_2^{(m)}(r,\theta),\ \tilde{\mathbf{F}}_3^{(m)}(r,\theta)\right] \tag{30a}$$

$$\widehat{\mathbf{F}}^{(m)}(r,\theta) = \left[\widehat{\mathbf{F}}_1^{(m)}(r,\theta),\ \widehat{\mathbf{F}}_2^{(m)}(r,\theta),\ \widehat{\mathbf{F}}_3^{(m)}(r,\theta)\right] \tag{30b}$$

where

$$\tilde{\mathbf{F}}_s^{(m)}(r,\theta)=\left[\tilde{F}_{s1}^{(m)}(r,\theta),\ \tilde{F}_{s2}^{(m)}(r,\theta),\ \tilde{F}_{s3}^{(m)}(r,\theta),\ \tilde{F}_{s4}^{(m)}(r,\theta)\right] \tag{31a}$$

$$\tilde{F}_{s1}^{(m)}(r,\theta)=\left(r\beta_s^{(m)}\right)^{\frac{1}{2}+\kappa}\cos\left(\rho_s^{(m)}\right),\quad \tilde{F}_{s2}^{(m)}(r,\theta)=\left(r\beta_s^{(m)}\right)^{\frac{1}{2}+\kappa}\sin\left(\rho_s^{(m)}\right) \tag{31b}$$

$$\tilde{F}_{s3}^{(m)}(r,\theta)=\left(r\beta_s^{(m)}\right)^{\frac{1}{2}-\kappa}\cos\left(\xi_s^{(m)}\right),\quad \tilde{F}_{s4}^{(m)}(r,\theta)=\left(r\beta_s^{(m)}\right)^{\frac{1}{2}-\kappa}\sin\left(\xi_s^{(m)}\right) \tag{31c}$$

$$\rho_s^{(m)}=\left(\frac{1}{2}+\kappa\right)\psi_s^{(m)},\quad \xi_s^{(m)}=\left(\frac{1}{2}-\kappa\right)\psi_s^{(m)},\quad s=1,2,3 \tag{31d}$$

and $\widehat{\mathbf{F}}_s^{(m)}(r,\theta)$ has the same form as Equation (29). As previously mentioned, for real singularity, $p_s^{(m)}$ with positive imaginary parts and their conjugates complex $\overline{p}_s^{(m)}$ will lead to identical enrichment functions; therefore, for this case only the eigenvalues with positive imaginary parts are involved. Similar to the ε-class problem, the numbers of enrichment functions for the elastic field and electric field are still different and special treatment should be applied to avoid the singularity of the system stiffness matrix.

In the following sections, our attention will be mainly focused on the ε-class problem, considering that the κ-class problem cannot be regarded as a new topic owing to the fact that, for the κ-class problem, no oscillating singularity is observed and its crack-tip enrichment functions are formally analogous to the existing ones for the homogeneous elastic materials [76] and piezoelectric materials [6, 8].

5. COMPUTATION OF *J*-INTEGRAL FOR INTERFACIAL CRACKS

The singular fields at the crack tip are usually characterized by stress intensity factors (SIFs) in the fracture mechanics of homogeneous materials. However, for interfacial crack problems in an elastic bimaterial and the ε-class piezoelectric bimaterial, the stresses near the crack tip exhibit the oscillating singularity. This is not realistic in practice. Therefore, researchers adopt the energy release rate (ERR) as the fracture parameter in fracture analysis for piezoelectric bimaterials [50, 55, 57]. In the fracture mechanics of linear piezoelectric materials, the ERR is equivalent to the path-

independent *J*-integral, which remains globally path independent for interface crack problems when there is no material inhomogeneity in the direction parallel to the crack [78]. Kuna [33, 72] has shown that the direct numerical determination of the *J*-integral is quite difficult owing to the fact that a contour or surface must be defined throughout the mesh for the accurate calculation of the integral. Therefore, the modified crack closure integral (MCCI) and equivalent domain integral are usually well suited to compute the ERR. MCCI can be utilized with both regular elements and special crack-tip elements, and has been extended to crack problems in homogeneous piezoelectricity [72]. One advantage of it is that the mechanical and electric ERRs can be calculated separately. However, the work concerning the application of MCCI to piezoelectric interface crack is very rare. This may be due to the presence of oscillating singularity, since some researchers have already observed that although the total ERR converges to a constant value, the individual components of ERRs do not exhibit steady values as the virtual crack extension tends to zero for an interface crack in elastic materials [79-81]. On the other hand, a transformation of the *J*-integral into an equivalent domain integral is much more favourable, which usually delivers the total ERR with the highest precision under both static and dynamic loadings [72]. Moreover, the equivalent domain integral also allows for an inherent error control because of its path independence. Therefore, herein we will adopt the equivalent domain integral to compute the *J*-integral.

The *J*-integral for piezoelectric cracked solids is defined as [6, 53]

$$J = \int_{\Gamma} \left(W\delta_{1j} - \sigma_{ij} u_{i,1} - D_j \phi_{,1} \right) n_j \mathrm{d}\Gamma, \quad i, j = 1,3 \tag{32}$$

where Γ is an arbitrary enclosing contour around the crack tip, starting from a point on the lower crack surface and terminating at a point on the upper crack surface; n_j is the *j*th component of the outward unit vector normal to it and *W* is the electric enthalpy density, which can be written as

$$W = \frac{1}{2}\left(\sigma_{ij}\varepsilon_{ij} - D_j E_j \right), \quad i, j = 1,3 \tag{33}$$

Applying the Gauss integral theorem, Equation (32) can be transformed to an equivalent domain expression

$$J = \int_A \left(\sigma_{ij} u_{i,1} + D_j \phi_{,1} - W \delta_{1j} \right) q_{,j} \mathrm{d}A + \int_A \left(\sigma_{ij} u_{i,1} + D_j \phi_{,1} - W \delta_{1j} \right)_{,j} q \mathrm{d}A, \quad i, j = 1,3 \tag{34}$$

where A is the area inside the contour Γ, and q is a smooth function, which assumes unity at nodes inside the domain A and zero at the nodes outside the domain. The value of q in any position of an element can be evaluated by the interpolation of the nodal values of q

$$q = \sum_i N_i q_i \tag{35}$$

The results of the J-integral are naturally independent of the integral path, but in the numerical calculation the accuracy may be affected by the integration path owing to the numerical error. Therefore, it is necessary to determine the proper integral path.

6. NUMERICAL EXAMPLES AND DISCUSSIONS

In this section, numerical examples of interfacial crack problems in a piezoelectric bimaterial are solved using X-FEM to validate the formulation. The first example corresponds to a Griffith interface crack under a combined far-field electromechanical uniform load. The analytical solution for this problem can be found in Suo et al. [43] and Herrman et al. [57]. The second example involves the interface crack between two bonded infinite strips and the analytical solution is given by Gu et al. [50]. Example 3 is an interface crack between two piezoelectric plates with finite size and the influence of the crack location on the fracture parameter is studied. In all the numerical examples, a piezoelectric bimaterial composed of piezoceramics $BaTiO_3$ and PZT-5H is used and the corresponding material constants are listed in Table I [48, 51]. With these material constants, the oscillating index ε is found as 0.0130 [48].

Moreover, in the present study, bilinear quadrilateral elements are used in all numerical examples. Since the interface crack is coincident with the element edges, no element partitioning is needed [77]. However, for the consideration of the accuracy in the numerical integration of the

weak form, the use of the high-order Gauss quadrature rule in the elements with an enriched degree of freedom is necessary [77]. We decompose the elements with the nodes enriched with the Heaviside function and the crack-tip enrichment functions into four quadrilaterals and, respectively, adopt 5×5 and 10×10 Gauss quadrature rules in each quadrilateral. A 2×2 Gauss quadrature rule is adopted in other non-enriched elements.

The convergence can be studied by comparing the analytical solution to a reference problem with the actual results of a numerical model; the error in the total energy norm is given by

$$\mathrm{err}_W = \sqrt{\frac{1}{2}\int\left[c_{ijkl}\left(\varepsilon_{ij}-\varepsilon_{ij}^{Ana}\right)\left(\varepsilon_{kl}-\varepsilon_{kl}^{Ana}\right)+\alpha_{ij}\left(E_i-E_i^{Ana}\right)\left(E_j-E_j^{Ana}\right)\right]\mathrm{d}V} \tag{36}$$

where ε_{ij}^{Ana} and E_i^{Ana} correspond to the analytical (exact) solution for elastic strains and electric fields, respectively. The convergence of error in the total energy norm with respect to mesh density has been thoroughly investigated in [6, 9, 82-84]. These all show that the convergence rate of topological enrichment is 0.5 whereas the geometrical one achieves a higher convergence rate, namely, 1.0. Therefore, in the present paper, we will no longer continue with the convergence rate study and instead the main focus will be on the accuracy study of X-FEM.

The following three subsections correspond to the aforementioned three examples, respectively. Figures 3 to 6 and Tables II to IV are related to the first example whereas Figure 3 and Table V correspond to the second example. Figures 7 and 8 refer to Example 3.

6.1. An interface crack between two semi-infinite piezoelectric planes

First, to validate the extended finite element implementation, an interface crack with the length $2a$ parallel to the x_1-axis between two dissimilar piezoelectric semi-infinite planes is considered. The crack is subject to a remote electromechanical load combination σ_0 and D_0 in the x_3 direction. The applied normal stress σ_0 is taken as 10 MPa and the loading combination parameter λ_D is taken as 2, which is introduced to reflect the applied electrical load and is defined as

$\lambda_D = c_{11}^{(1)} D_0 \big/ e_{33}^{(1)} \sigma_0$. If no special explanation is given, this load combination will always be adopted. Under the aforementioned load combination, the analytical result of the normalized *J*-integral $J^{Ana} \big/ a\sigma_0$ for this problem is equal to 2.7863×10^{-4} [57].

Considering the symmetry, only half of the specimen is considered, as shown in Figure 3a, and the horizontal displacement on the left-hand edge of the half model is set as zero. The sample size is firstly taken as $w = 20a$ and $2h = 40a$ to model the infinite domain, and in the following numerical results we will show this assumption is reasonable. Figure 3b shows the uniform finite element mesh with $h_e = a/10$ in the vicinity of the crack, where h_e denotes the element size. A numerical investigation is conducted in detail, with the following objectives:

(i) To study domain independence and the influence of the element size on the *J*-integral;

(ii) To compare the performance of topological enrichment and geometrical enrichment as well as the performance of new enrichment functions (Equations (27) and (28), and the standard isotropic enrichment functions, i.e. Equation (13));

(iii) To explore finite size specimen effects and trends on the *J*-integral;

(iv) To study the robustness of the present method for small perturbations of the crack tip；

(v) To compare the accuracy of results obtained on uniform mesh and non-uniform mesh with local refinement.

Considering the material mismatch in the interface crack problem, the domain independence study for determining an appropriate domain radius is necessary to achieve good accuracy of the *J*-integral. This study is very meaningful since, to date, it has not been carried out in relation to the interface crack problem in piezoelectric bimaterial. In Figure 4, results of the domain independence study are presented, where r_k is a scalar multiple used to define the domain radius r_d by $r_d = r_k h_e$. Two different uniform meshes, $h_e = a/6$ and $h_e = a/10$, are adopted, respectively corresponding to 120×240 and 200×400 elements. Moreover, six enrichment strategies are employed, including

topological and geometrical enrichments based on the newly derived crack-tip enrichment functions and standard isotropic enrichment functions. The results in Figure 4 demonstrate that for all the aforementioned enrichment strategies, the *J*-integral obtained by X-FEM tends to be a converged value as $r_k \geq 4$. This is in agreement with the results of Sukumar et al. [77] in relation to the interface crack problem in isotropic elastic bimaterials. Therefore, in the following computation, if no special explanation is given, r_k is taken as 5. Certainly, some researchers adopt more conservative values; for example Béchet et al. [6] and Bhargava and Sharma [7] used $r_k = 0.8a$.

Figure 5 describes the convergence of the *J*-integral by plotting the relationship between the mesh density and the error percentage of the *J*-integral in a log-log scale. As expected, with the increase in mesh density, the error decreases rapidly and a high accuracy is available with a relative coarse finite element mesh. The results in Figures 4 and 5 show that the geometrical enrichment achieves a higher accuracy than the topological enrichment. The geometrical enrichment with a larger radius of enriched domain performs better than that with a small one. All these phenomena are consistent with those previously observed in homogeneous piezoelectric materials [6] and magnetoelectroelastic materials [82, 83]. Moreover, the accuracy of the new crack-tip enrichment functions specifically derived for piezoelectric bimaterials is superior to that of the standard isotropic ones if the same topological and/or geometrical enrichment is employed. Additionally, comparison between the results obtained by the X-FEM and those obtained by classical FEM without enrichment is made, and obviously the former is greatly superior to the latter.

Since the reference solution is related to the infinite domain problem, we also study the finite specimen effects for different enrichment strategies as $h_e = a/10$ and the results are presented in Table II. As expected, as the ratio of w/a increases, the *J*-integral decreases. As $w/a \geq 20$ ($h = w$), variations of the *J*-integral are extremely small and negligible for all enrichment strategies. Therefore, using the domain size of $40a$ to model the infinite domain is acceptable.

To investigate the robustness of the present method, a simple test is carried out and corresponding results are listed in Table III. The specimen and mesh parameters are also $w = 20a$, $2h = 40a$, $h_e = a/10$ and $r_k = 5$, assuming that the location of the crack tip is perturbed by $\pm\Delta/a = \pm 0.001$ [77], and the results are compared with those for $\Delta = 0$. Similar to previous numerical examples, six different enrichment strategies are employed. From Table III, we observe that for small perturbations, the *J*-integrals are stable for all enrichment strategies.

In classical FEM, local refinement of the meshes near the crack tip is a commonly used method for improving computational accuracy. In the present work, we also investigate the efficiency and accuracy of uniform mesh and non-uniform mesh with local refinement. As shown in Figure 6, h_e^1 and h_e^2 are, respectively, the mesh sizes of elements in the vicinity of the crack tip and far away from the crack tip, and h_e^1 is much smaller than h_e^2. Herein the mesh with size h_e^1 is only applied to the domain composed of $x \in [0,\ 2a]$ and $y \in [-a,\ a]$. A similar mesh was also adopted by Asadpoure and Mohammadi [76] to perform the X-FEM analysis for crack problems in orthotropic solids. Certainly, the uniform mesh herein is less efficient than the graded mesh [33, 72], but one advantage of it is that its mesh generation is simpler than the latter. In Table IV we compare the element numbers and computational accuracy of uniform mesh and non-uniform mesh for different mesh densities and enrichment strategies. The results in Table IV reveal that the non-uniform mesh achieves a high accuracy with a less number of elements. As previously shown in Figures 4 and 5, if the same enrichment strategy is adopted, the accuracy of new crack-tip enrichment functions is better than that of standard isotropic enrichment functions. Moreover, by refining the meshes near the crack tips and using a large enriched radius, the geometrical isotropic enrichment can also achieve high accuracy.

6.2. An interface crack between two bonded infinite piezoelectric strips

In this example, an interface crack between two infinite piezoelectric strips is analysed. The load boundary conditions are the same as for the previous example, i.e. $\sigma_0 = 10\,\text{MPa}$ and $\lambda_D = 2$. As shown in Figure 3, the width of half model $w = 20a$ is also taken to model the strips with infinite length and the height of each layer h is taken as a much smaller value. The analytical solution to this problem can be readily obtained from Gu et al. [50] by setting the applied load independent of time. According to the results presented in the first example, herein we only adopt the non-uniform mesh, i.e. $h_e^1 = a/20$ and $h_e^2 = a/4$, which costs less computational time. Results of the *J*-integral obtained by the analytical solution and the X-FEM for different heights of the strips are given in Table V. It is found that the *J*-integral solved by the X-FEM is always in excellent agreement with the analytical solution. Table V and Figure 5 again demonstrate that, although a specific enrichment scheme with standard isotropic enrichment functions produces a good approximation with less computational cost, it remains slightly inferior to the corresponding one with the new crack-tip enrichment functions specially derived for piezoelectric bimaterials when compared with the analytical results.

6.3. An interface crack between two bonded piezoelectric plates

As shown in Figure 7, an interface crack of arbitrary location between two finite piezoelectric plates is considered. The load boundary conditions are same as in the previous examples, i.e. $\sigma_0 = 10\,\text{MPa}$ and $\lambda_D = 2$. The specimen parameters are as follows: the square plate width is $20a$ and the heights of upper and lower plates $h = 10a$. The left and right crack tips are, respectively, denoted by *A* and *B*. The distance between the crack centre and interface centre is denoted by *d*. Similarly, we still adopt the non-uniform mesh, $h_e^1 = a/20$, $h_e^2 = a/4$ and the mesh with size h_e^1 is only applied to the domain composed of $x \in [d-2a,\, d+2a]$ and $y \in [-a,\, a]$. Moreover, for comparison the results obtained by classical FEM with the mesh $h_e^1 = a/200$, $h_e^2 = a/4$ are also

provided. The domain radius factor r_k is taken as 10. The influence of the location of the interface crack on the *J*-integrals at the left and right crack tips is examined and the numerical results are plotted in Figure 8. It is found that with the increasing of *d*, the *J*-integral at both the left crack tip J_A and the right crack tip J_B increase, especially as the right crack tip approaches the right edge of the plate. This is consistent with our expectations. Again, the difference in results among the X-FEM based on new enrichment functions, the standard isotropic enrichment functions and the classic FEM is slight, at less than 0.4%.

From the aforementioned three numerical examples, it is demonstrated that high accuracy can be achieved with relatively coarse meshes, especially when the newly derived crack-tip enrichment functions are adopted in the X-FEM.

6. CONCLUDING REMARKS

An extended finite element method (X-FEM) formulation for the fracture analysis of interface cracks between two dissimilar transversely isotropic piezoelectric materials is presented. Corresponding to two classes of singularities of the aforementioned problem, namely ε class and κ class, two classes of crack-tip enrichment functions are newly derived by referring to the analytic solution. As a completely new topic, the ε class problem is numerically analyzed by means of the X-FEM under plane strain conditions. The validity of the X-FEM analysis on interface crack problems in a piezoelectric bimaterial is verified by showing that the X-FEM results of the *J*-integral for several crack configurations are in excellent agreement with the existing analytical and numerical solutions. Two enrichment strategies, namely topological enrichment and geometrical enrichment, as well as two kinds of mesh, namely uniform mesh and non-uniform mesh with local refinement, are adopted in numerical examples. It is found that the geometrical enrichment in connection with the non-uniform mesh is substantially better in terms of accuracy and efficiency. Additionally, the numerical tests indicate that although the geometrical enrichment

with a large enriched domain based on the simpler isotropic enrichment functions can produce a good approximation for the interface crack problem in piezoelectric bimaterials, the newly derived crack-tip enrichment functions lead to the most accurate results.

ACKNOWLEDGEMENTS

Support from the National Natural Science Foundation of China (Grant Nos. 10772123 and 11072160), and the Training Program for Leading Talent in University Innovative Research Team in Hebei Province (LJRC006) is gratefully acknowledged. The authors also appreciate the valuable comments and suggestions given by the anonymous reviewers for the improvement of the paper.

REFERENCES

1. Belytschko T, Black T. Elastic crack growth in finite elements with minimal remeshing. *International Journal for Numerical Methods in Engineering* 1999; **45**:601-620.
2. Yazid A, Abdelmadjid H. A survey of the extended finite element. *Computer and Structures* 2008; **86**:1141-1151.
3. Yazid A, Abdelkader N, Abdelmadjid H. A state-of-the-art review of the X-FEM for computational fracture mechanics. *Applied Mathematical Modelling* 2009; **33**:4269-4282.
4. Mohammadi S. *Extended finite element method for fracture analysis of structures*. Blackwell Publishing Ltd, 2008.
5. Zhuang Z, Liu Z, Cheng B, Liao J. *Extended finite element method*. Elsevier/Tsinghua University Press, Beijing, 2014.
6. Béchet E, Scherzer M, Kuna M. Application of the X-FEM to the fracture of piezoelectric materials. *International Journal for Numerical Methods in Engineering* 2009; **77**:1535-1565.
7. Bhargava RR, Sharma K. A study of finite size effects on cracked 2-D piezoelectric media using extended finite element method. *Computational Materials Science* 2011; **50**:1834-1845.
8. Bhargava RR, Sharma K. X-FEM simulation for two-unequal-collinear cracks in 2-D finite piezoelectric specimen. *International Journal of Mechanics and Materials in Design* 2012, 8, 129-148.
9. Sharma K, Bui TQ, Zhang C, Bhargava RR. Analysis of a subinterface crack in piezoelectric bimaterials with the extended finite element method. *Engineering Fracture Mechanics* 2013; **104**:114-139.
10. Liu P, Yu T, Bui TQ, Zhang C. Transient dynamic crack analysis in non-homogeneous functionally graded piezoelectric materials by the X-FEM. *International Journal of Solids and Structures* 2013; **69**: 542–558.
11. Liu P, Yu T, Bui TQ, Zhang C, Xu Y, Lim CW. Transient thermal shock fracture analysis of functionally graded piezoelectric materials by the extended finite element method. *International Journal of Solids and Structures* 2014; **51**: 2167–2182.
12. Nguyen-Vinh H, Bakar I, Msekh M, Song JH, Muthu J, Zi G, Le P, Bordas S, Simpson R, Natarajan S, Lahmer T, Rabczuk T. Extended finite element method for dynamic fracture of piezo-electric materials. *Engineering Fracture Mechanics* 2012; **92**: 19-31.
13. Bui TQ, Zhang C. Extended finite element simulation of stationary dynamic cracks in piezoelectric solids under impact loading. *Computational Material Science* 2012; **62**: 243-257.

14. Nanthakumar SS, Lahmer T, Rabczuk T. Detection of multiple flaws in piezoelectric structures using XFEM and level sets. *Computer Methods in Applied Mechanics and Engineering* 2014; **275**: 98–112.
15. Nanthakumar SS, Lahmer T, Rabczuk T. Detection of flaws in piezoelectric structures using extended FEM. *International Journal for Numerical Methods in Engineering* 2013; **96**: 373-389.
16. Barsoum RS. On the use of isoparametric finite elements in linear fracture mechanics. *International Journal for Numerical Methods in Engineering* 1976; **10**: 25-37.
17. Simo JC, Oliver J, Armero F. An analysis of strong discontinuities induced by strain-softening in rate-independent inelastic solids. *Computational Mechanics* 1993; **12**: 277-296.
18. Armero F, Garikipati K. An analysis of strong discontinuities in multiplicative finite strain plasticity and their relation with the numerical simulation of strain localization in solids. *International Journal of Solids and Structures* 1996; **33**: 2863-2885.
19. Borja R. A finite element model for strain localization analysis of strongly discontinuous fields based on standard Galerkin approximation. *Computer Methods in Applied Mechanics and Engineering* 2000; **190**: 1529-1549.
20. Oliver J, Huespe AE, Pulido MDG, Samaniego E. On the strong discontinuity approach in finite deformation settings. *International Journal for Numerical Methods in Engineering* 2003; **56**: 1051-1082.
21. Radulovic R, Bruhns OT, Mosler J. Effective 3d failure simulations by combining the advantages of embedded strong discontinuity approaches and classical interface elements. *Engineering Fracture Mechanics* 2011; **78**: 2470-2485.
22. Armero F, Linder C. Numerical simulation of dynamic fracture using finite elements with embedded discontinuities. *International Journal Fracture* 2009; **160**: 119-141.
23. Linder C, Raina A. A strong discontinuity approach on multiple levels to model solids at failure. *Computer Methods in Applied Mechanics and Engineering* 2013; **253**: 558-583.
24. Rabczuk T, Belytschko T. Cracking particles: a simplified meshfree method for arbitrary evolving cracks. *International Journal for Numerical Methods in Engineering* 2004; **61**: 2316-2343.
25. Rabczuk T, Belytschko T. A three-dimensional large deformation meshfree method for arbitrary evolving cracks. *Computer Methods in Applied Mechanics and Engineering* 2007; **196**: 2777-2799.
26. Rabczuk T, Samaniego E. Discontinuous modelling of shear bands using adaptive meshfree methods. *Computer Methods in Applied Mechanics and Engineering* 2008; **197**: 641-658.

27. Rabczuk T, Song JH, Belytschko T. Simulations of instability in dynamic fracture by the cracking particles method. *Engineering Fracture Mechanics* 2009; **76**: 730-741.
28. Rabczuk T, Zi G, Bordas S. A simple and robust three-dimensional cracking-particle method without enrichment. *Computer Methods in Applied Mechanics and Engineering* 2010; **199**: 2437-2455.
29. Miehe C, Hofacker M, Welschinger F. A phase field model for rate-independent crack propagation: Robust algorithmic implementation based on operator splits. *Computer Methods in Applied Mechanics and Engineering* 2010; **199**: 2765-2778.
30. Miehe C, Welschinger F, Hofacker M. Thermodynamically consistent phase-field models of fracture: variational principles and multi-field FE implementations. *International Journal for Numerical Methods in Engineering* 2010; **83**: 1273-1311.
31. Kumar S, Singh RN. Crack propagation in piezoelectric materials under combined mechanical and electrical loadings. *Acta Materialia* 1996; **44**: 173-200.
32. Kuna M. FEM-Techniken zur Analyse von Rissen unter elektrischen und mechanischen Beanspruchungen, Berichte 29. Tagung DVM Arbeitskreis Bruchvorgänge, 1997; 369–379.
33. Kuna, M. Finite element analyses of crack problems in piezoelectric structures. *Computational Materials Science* 1998; **13**: 67-80.
34. Kuna M, Ricoeur, A. Theoretical investigations on the cracking of ferroelectric ceramics. In: *Smart Structures and Materials 2000: Active Materials Behavior and Mechanics, Proceedings of SPIE* 2000; **3992**, 185-196.
35. Linder C, Rosato D, Miehe C. New finite elements with embedded strong discontinuities for the modeling of failure in electromechanical coupled solids. *Computer Methods in Applied Mechanics and Engineering* 2011; **200**: 141-161.
36. Linder C, Miehe C. Effect of electric displacement saturation on the hysteretic behavior of ferroelectric ceramics and the initiation and propagation of cracks in piezoelectric ceramics. *Journal of the Mechanics and Physics of Solids* 2012; **60**: 882–903.
37. Linder C. An analysis of the exponential electric displacement saturation model in fracturing piezoelectric ceramics. *Technische Mechanik* 2012; **32**: 53-69.
38. Linder C, Zhang X. Three-dimentional finite elements with embedded strong discontinuities to model failure in electromechanical coupled materials. *Computer Methods in Applied Mechanics and Engineering* 2014; **273**: 143-160.
39. Miehe C, Welschinger F, Hofacker M. A phase field model of electromechanical fracture. *Journal of the Mechanics and Physics of Solids* 2010; **58**, 1716-1740.

40. Abdollahi A, Arias I. Phase-field modeling of crack propagation in piezoelectric and ferroelectric materials with different electromechanical crack conditions. *Journal of the Mechanics and Physics of Solids* 2012; **60**: 2100-2126.
41. Wilson Z, Borden M, Landis CM. A phase-field model for fracture in piezoelectric ceramics. *International Journal Fracture* 2013;**183**, 135-153.
42. Kuo CM, Barnett DM. Stress singularities of interfacial cracks in bonded piezoelectric half-spaces. *Modern Theory of Anisotropic Elasticity and Applications*, Philadelphia, 1991.
43. Suo Z, Kuo CM, Barnett DM. Fracture mechanics for piezoelectric ceramics. *Journal of the Mechanics and Physics of Solids* 1992; **40**:739-765.
44. Beom HG, Atluri SN. Near-tip fields and intensity factors for interfacial cracks in dissimilar anisotropic piezoelectric media. *International Journal of Fracture* 1996; **75**, 163-183.
45. Qin QH, Mai YW. A closed crack tip model for interface cracks in thermopiezoelectric materials. *International Journal of Solids and Structures* 1999; **36**: 2463-2479.
46. Gao CF, Wang MZ. Collinear permeable cracks in thermopiezoelectric materials. *Mechanics of Materials* 2001; **33**:1-9.
47. Beom HG, Atluri SN. Conducting cracks in dissimilar piezoelectric media. *International Journal of Fracture* 2002; **118**, 285-301.
48. Ou ZC, Wu XJ. On the crack-tip stress singularity of interfacial cracks in transversely isotropic piezoelectric bimaterials. *International Journal of Solids and Structures* 2003; **40**: 7499-7511.
49. Ma LF, Chen YH. Weight functions for interface cracks in dissimilar anisotropic piezoelectric materials. *International Journal of Fracture* 2001; **110**, 263-279.
50. Gu B, Yu SW, Feng XQ. Transient response of an interface crack between dissimilar piezoelectric layers under mechanical impacts. *International Journal of Solids and Structures* 2002; **39**: 1743-1756.
51. Ou ZC. Singularity parameters epsilon and kappa for interface cracks in transversely isotropic piezoelectric biomaterials. *International Journal of Fracture* 2003; **119**, L41-L46.
52. Wang X, Zhong Z, Wu FL. A moving conducting crack at the interface of two dissimilar piezoelectric materials. *International Journal of Solids and Structures* 2003; **40**: 2381-2399.
53. Gao CF, Hausler C, Balke H. Periodic permeable interface cracks in piezoelectric materials. *International Journal of Solids and Structures* 2004; **41**: 323-335.
54. Govorukha VB, Loboda VV, Kamlah M. On the influence of the electric permeability on an interface crack in a piezoelectric bimaterial compound. *International Journal of Solids and Structures* 2006; **43**: 1979-1990.

55. Li Q, Chen YH. Solution for a semi-permeable interface crack between two dissimilar piezoelectric materials. *ASME Journal of Applied Mechanics* 2007; **74**: 833-844.
56. Lapusta Y, Komarov A, Labesse-Jied F, Moutou Pitti R, Loboda V. Limited permeable crack moving along the interface of a piezoelectric bi-material. *European Journal of Mechanics A-Solids* 2011; **30**: 639-649.
57. Herrmann KP, Loboda VV, Govorukha VB. On contact zone models for an electrically impermeable interface crack in a piezoelectric biomaterial. *International Journal of Fracture* 2001; **111**, 203-227.
58. Herrmann KP, Loboda VV. Fracture mechanical assessment of interface cracks with contact zones in piezoelectric bimaterials under thermoelectromechanical loadings II. Electrically impermeable interface cracks. *International Journal of Solids and Structures* 2003; **40**: 4219-4237.
59. Govorukha V, Kamlah M, Munz D. The interface crack problem for a piezoelectric semi-infinite strip under concentrated electromechanical loading. *Engineering Fracture Mechanics* 2004; **71**:13-14.
60. Loboda V, Lapusta Y, Sheveleva A. Electro-mechanical pre-fracture zones for an electrically permeable interface crack in a piezoelectric bimaterial. *International Journal of Solids and Structures* 2007; **44**: 5538-5553.
61. Liew KM, Liang J. Modeling of 3D transversely piezoelectric and elastic bimaterials using the boundary element method. *Computational Mechanics* 2002; **29**:151-162.
62. Guo XH, Fang DN. Simulation of interface cracking in piezoelectric layers. *International Journal of Nonlinear Sciences and Numerical Simulation* 2004; **5**: 235-242.
63. Govorukha V, Kamlah M. Asymptotic fields in the finite element analysis of electrically permeable interface cracks in piezoelectric bimaterials. *Archive of Applied Mechanics* 2004; **74**:92-101.
64. Govorukha V, Kamlah M. An analytically-numerical approach for the analysis of an interface crack with a contact zone in a piezoelectric bimaterial compound. *Archive of Applied Mechanics* 2008; **78**:575-586.
65. Scherzer M, Kuna M. Combined analytical and numerical solution of 2D interface corner configurations between dissimilar piezoelectric materials. *International Journal of Fracture* 2004; **127**, 61-99.
66. Benedetti I, Aliabadi MH, Milazzo AA. Fast BEM for the analysis of damaged structures with bonded piezoelectric sensors. *Computer Methods in Applied Mechanics and Engineering* 2010; **199**, 490-504.

67. Sladek J, Sladek V, Zhang C., Garcia-Sanchez F., Wüensche M. Meshless local Petrov–Galerkin method for plane piezoelectricity. *Computers Materials and Continua* 2006; **4**,109-118.
68. Sladek J, Sladek V, Wüensche M, Zhang C. Analysis of an interface crack between two dissimilar piezoelectric solids. *Engineering Fracture Mechanics* 2012; **89**:114-127.
69. Lei J, Zhang C. Time-domain BEM for transient interfacial crack problems in anisotropic piezoelectric bi-materials. *International Journal of Fracture* 2012; **174**, 163-175.
70. Lei J, Garcia-Sanchez F, Zhang C. Determination of dynamic intensity factors and time-domain BEM for interfacial cracks in anisotropic piezoelectric materials. *International Journal of Solids and Structures* 2013; **50**: 1482-1493.
71. Li C, Song C, Man H, Ooi ET, Gao W. 2D dynamic analysis of cracks and interface cracks in piezoelectric composites using the SBFEM. *International Journal of Solids and Structures* 2014; **51**: 2096-2108.
72. Kuna M. Finite element analyses of cracks in piezoelectric structures: a survey. *Archive of Applied Mechanics* 2006; **76**: 725-745.
73. Kuna M. Fracture mechanics of piezoelectric materials–Where are we right now? *Engineering Fracture Mechanics* 2010; **77**: 309-326.
74. Laborde P, Pommier J, Renard Y, Salaün M. High-order extended finite element method for cracked domains. *International Journal for Numerical Methods in Engineering* 2005; **64**:1033-1056.
75. Fang D, Liu J. *Fracture Mechanics of Piezoelectric and Ferroelectric Solids*. Springer Berlin Heidelberg, 2013.
76. Asadpoure A, Mohammadi S. Developing new enrichment functions for crack simulation in orthotropic media by the extended finite element method. *International Journal for Numerical Methods in Engineering* 2007; **69**:2150-2172.
77. Sukumar N, Huang ZY, Prévost J-H, Suo Z. Partition of unity enrichment for bimaterial interface cracks. *International Journal for Numerical Methods in Engineering* 2004; **59**:1075-1102.
78. Smelser RE. On the *J*-integral for bi-material bodies. *International Journal of Fracture* 1977; **13**: 382-384.
79. Sun CT, Jih CJ. On strain energy release rates for an interfacial crack in bimaterial media. *Engineering Fracture Mechanics* 1987; **28**, 13-20.
80. Raju IS, Crews JH, Aminpour MA. Convergence of strain energy release rate components for edge delaminated composite laminates. *Engineering Fracture Mechanics* 1988; **30**: 383-396.

81. Sun CT, Manoharan MG. Strain energy release rates of an interfacial cracks between two orthotropic solids. *Journal of Composite Materials* 1989; **23**: 460-478.
82. Rojas-Díaz R, Sukumar N, Sáez A, García-Sánchez F. Fracture in magnetoelectroelastic materials using the extended finite element. *International Journal for Numerical Methods in Engineering* 2011; **88**:1238-1259.
83. Bhargava RR, Sharma K. Application of X-FEM to study two-unequal-collinear cracks in 2-D finite magnetoelectroelastic specimen. *Computational Materials Science* 2012; **60**:75-98.
84. Hattori G, Rojas-Díaz R, Sáez A, Sukumar N, García-Sánchez F. New anisotropic crack-tip enrichment functions for the extended finite element method. *Computational Mechanics* 2012; **50**:591-601.

Figure and table captions

Figure 1. An interface crack in a piezoelectric bimaterial.

Figure 2. Enriched nodes for a bimaterial interface crack: (a) topological enrichment; (b) geometrical enrichment (the nodes enriched by the Heaviside function are marked with open circles whereas the nodes enriched by crack-tip enrichment functions are marked with filled circles).

Figure 3. Interface crack under electromechanical load (half -model): (a) problem configuration; (b) uniform mesh in the vicinity of the crack ($h_e = a/10$).

Figure 4. Domain independence study for interface crack: (a) $h_e = a/6$; (b) $h_e = a/10$.

Figure 5. Convergency study of the *J*-integral with respect to mesh density for interface crack.

Figure 6. The non-uniform mesh with local refinement in the vicinity of the crack: $h_e^1 = a/20$, $h_e^2 = a/4$.

Figure 7. An interface crack between two finite piezoelectric plates.

Figure 8. Normalized *J*-integral with respect to the location of interface crack.

Table I. Material properties of piezoelectrics $BaTiO_3$ and PZT-5H [48, 51] (c_{ij} in 10^9 N/m^2, e_{ij} in C/m^2, ε_{ij} in 10^{-9}C/Vm).

Table II. Finite specimen effects for interface crack in terms of error $\left(J^{Ana.} - J\right)/J^{Ana.}(\%)$ ($h_e = a/10$).

Table III. Robustness study for interface crack in terms of error $\left(J^{Ana.} - J\right)/J^{Ana.}(\%)$ ($h_e = a/10$).

Table IV. Comparison of element number and error $\left(J^{Ana.} - J\right)/J^{Ana.}(\%)$ between uniform mesh and non-uniform mesh for interface crack.

Table V. Convergency study of the *J*-integral in terms of error $\left(J^{Ana.} - J\right)/J^{Ana.}(\%)$ with respect to the height of piezoelectric layers ($h_e^1 = a/20$, $h_e^2 = a/4$).

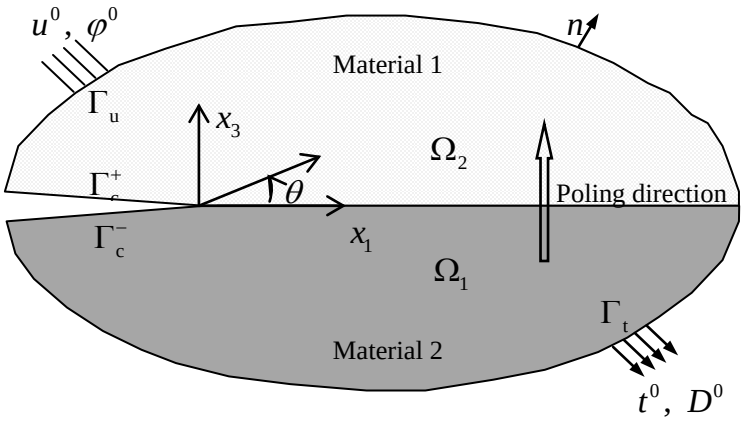

Figure 1. An interface crack in a piezoelectric bimaterial.

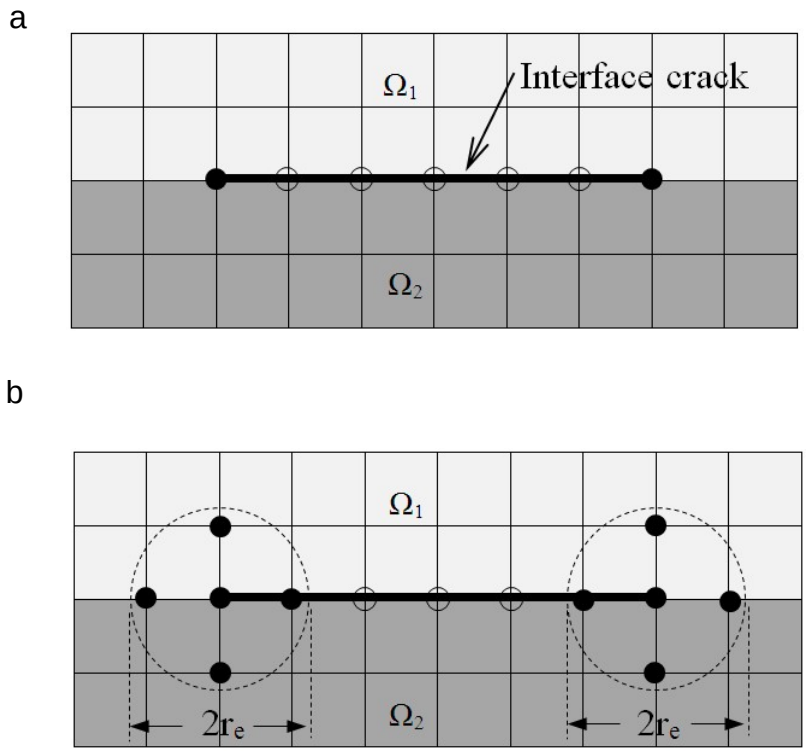

Figure 2. Enriched nodes for a bimaterial interface crack: (a) topological enrichment; (b) geometrical enrichment (the nodes enriched by the Heaviside function are marked with open circles whereas the nodes enriched by crack-tip enrichment functions are marked with filled circles).

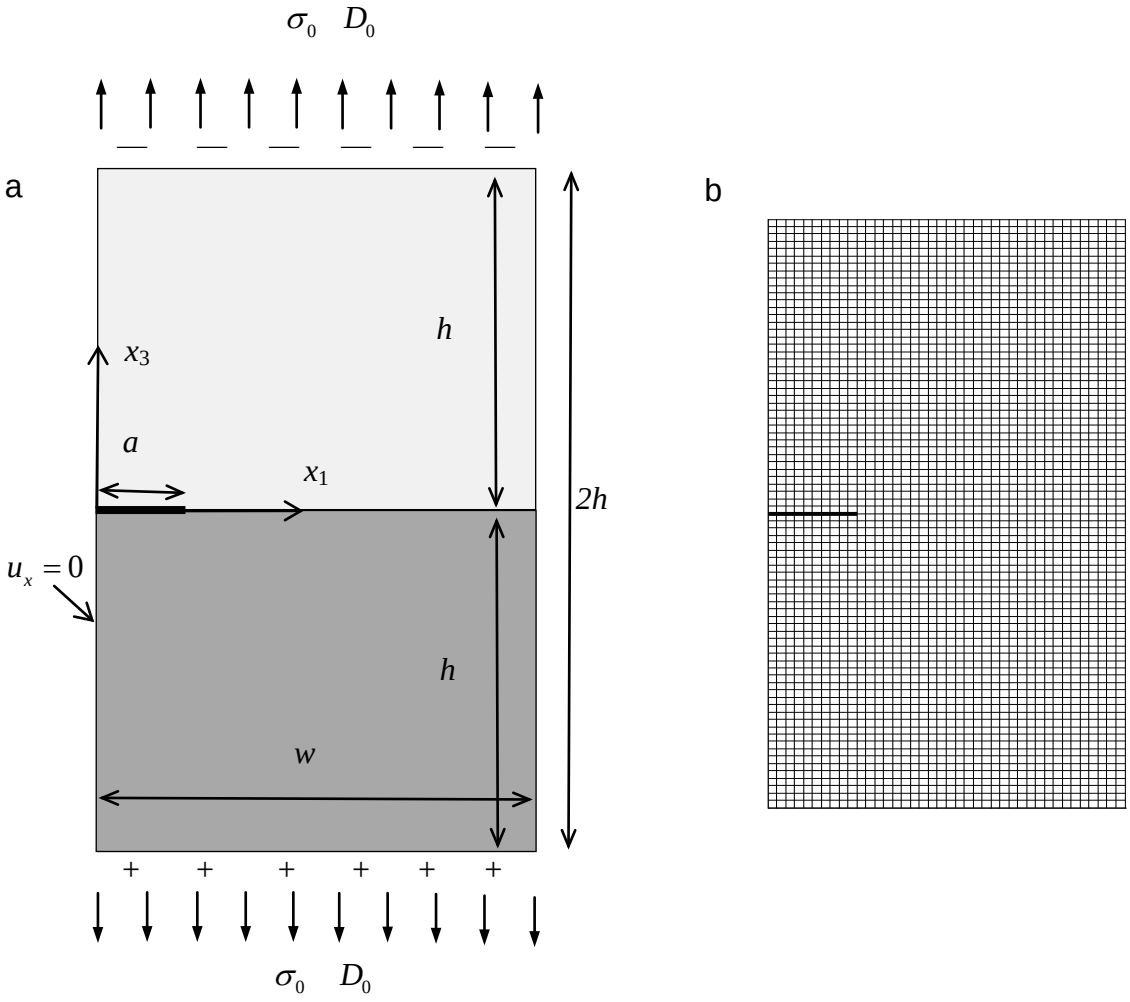

Figure 3. Interface crack under electromechanical load (half -model): (a) problem configuration; (b) uniform mesh in the vicinity of the crack ($h_e = a/10$).

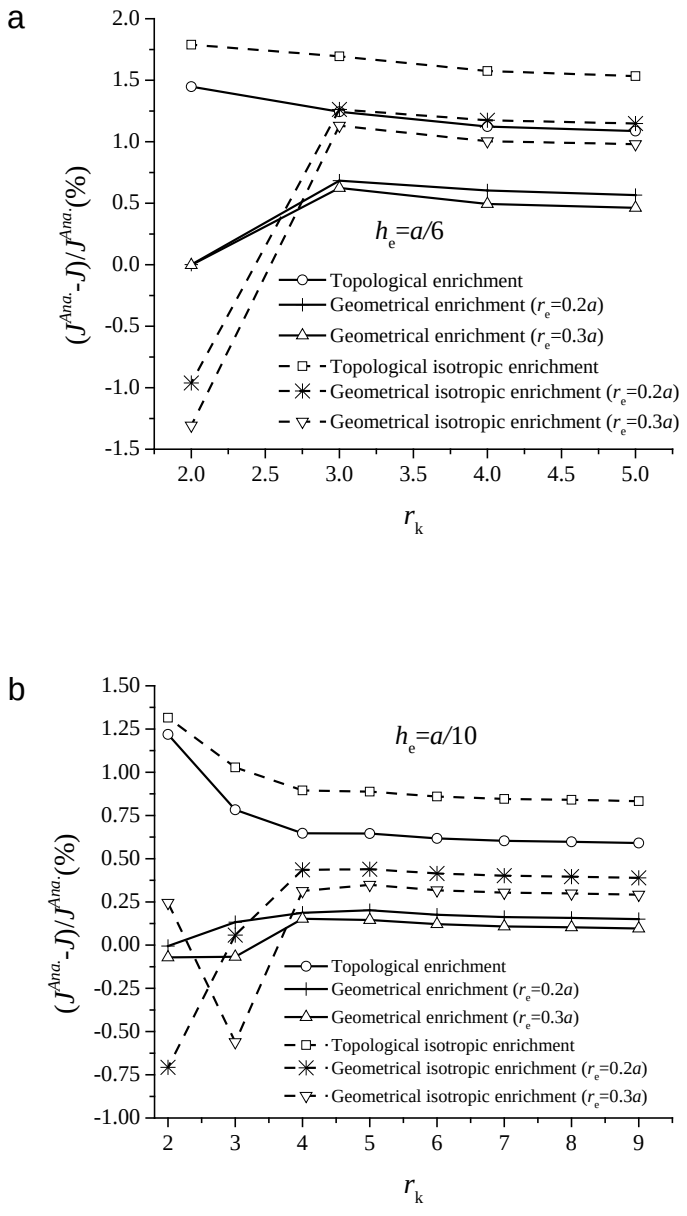

Figure 4. Domain independence study for interface crack: (a) $h_e = a/6$; (b) $h_e = a/10$.

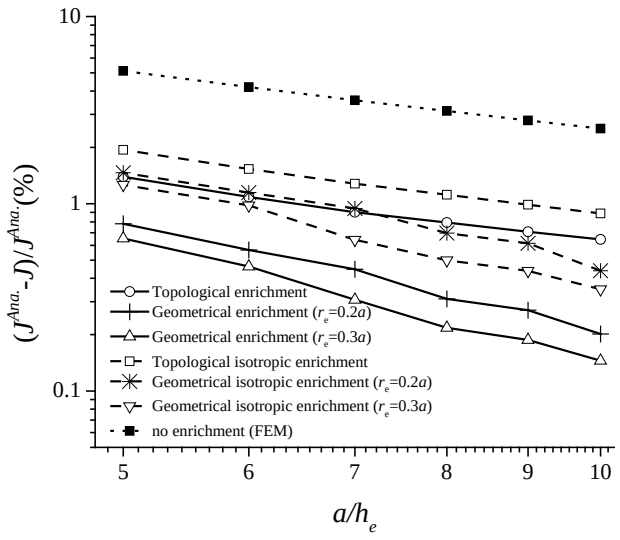

Figure 5. Convergency study of the *J*-integral with respect to mesh density for interface crack.

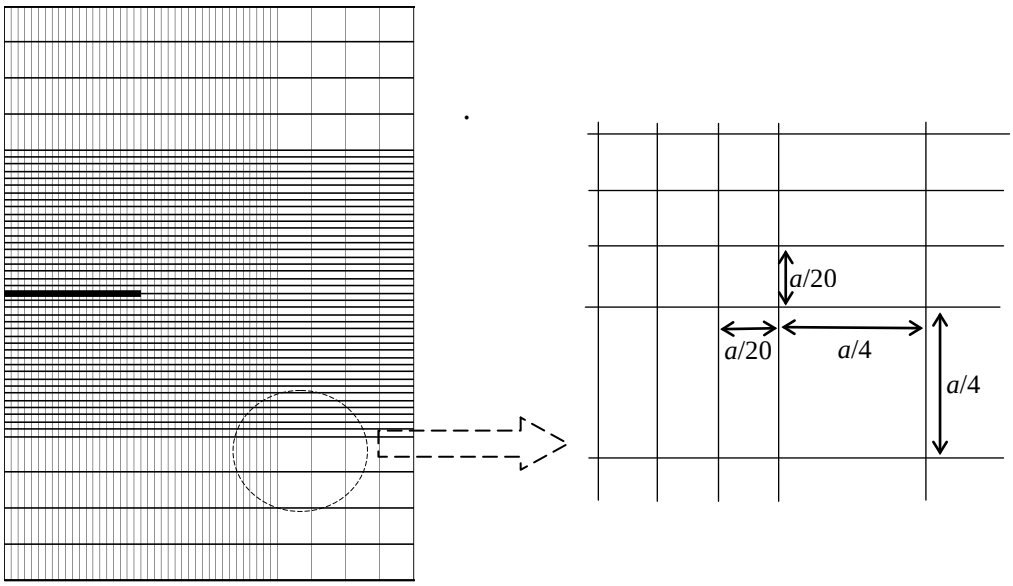

Figure 6. The non-uniform mesh with local refinement in the vicinity of the crack: $h_e^1 = a/20\,, h_e^2 = a/4\,.$

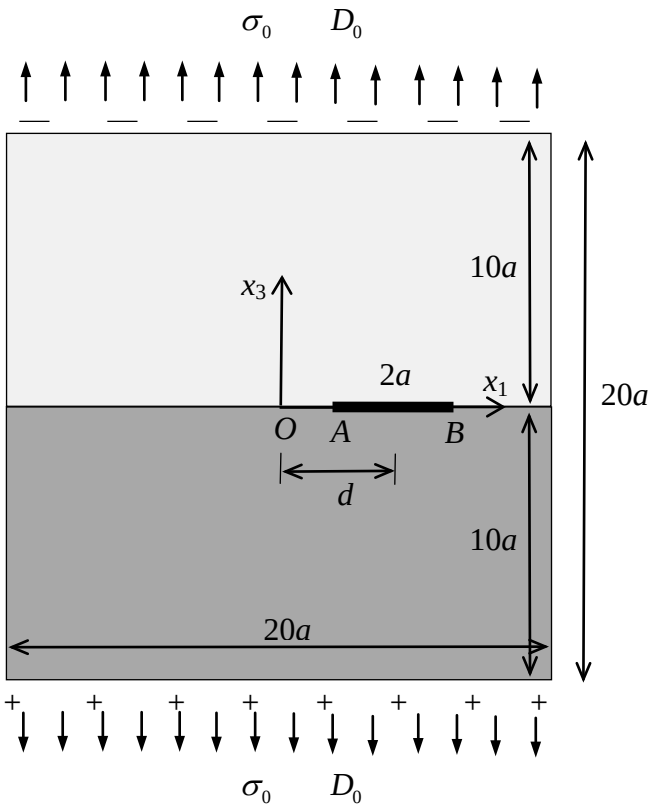

Figure 7. An interface crack between two finite piezoelectric plates.

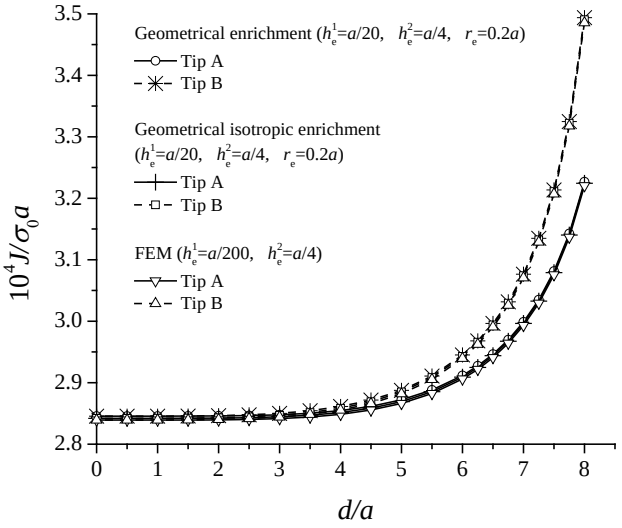

Figure 8. Normalized *J*-integral with respect to the location of interface crack.

Table I. Material properties of piezoelectrics $BaTiO_3$ and PZT-5H [48, 51]
(c_{ij} in 10^9 N/m^2, e_{ij} in C/m^2, ε_{ij} in 10^{-9}C/Vm).

	c_{11}	c_{13}	c_{33}	c_{44}	e_{15}	e_{31}	e_{33}	ε_{11}	ε_{33}
$BaTiO_3$	150	66	146	44	11.4	-4.35	17.5	9.87	11.2
PZT-5H	126	53	117	35.3	17.0	-6.50	23.3	15.1	13.0

Table II. Finite specimen effects for interface crack in terms of error $\left(J^{Ana.}-J\right)/J^{Ana.}(\%)$ ($h_e = a/10$).

w/a ($h=w$)	Topological enrichment	Geometrical enrichment ($r_e = 0.2a$)	Geometrical enrichment ($r_e = 0.3a$)	Topological isotropic enrichment	Geometrical isotropic enrichment ($r_e = 0.2a$)	Geometrical isotropic enrichment ($r_e = 0.3a$)
5	-9.2604	-9.7657	-9.8738	-8.9068	-9.4399	-9.6272
10	-1.5518	-1.9905	-2.0508	-1.2647	-1.7411	-1.8348
15	0.3125	-0.1177	-0.1858	0.5715	0.1197	0.0313
20	0.6454	0.2015	0.1358	0.8880	0.4390	0.3492
25	0.8023	0.3419	0.2765	1.0256	0.5785	0.4891

Table III. Robustness study for interface crack in terms of error $\left(J^{Ana.}-J\right)/J^{Ana.}(\%)$ ($h_e = a/10$).

Δ/a	Topological enrichment	Geometrical enrichment ($r_e = 0.2a$)	Geometrical enrichment ($r_e = 0.3a$)	Topological isotropic enrichment	Geometrical isotropic enrichment ($r_e = 0.2a$)	Geometrical isotropic enrichment ($r_e = 0.3a$)
0	0.6454	0.2015	0.1452	0.8880	0.4390	0.3492
-0.001	0.6961	0.2516	0.1887	0.9792	0.5654	0.4562
0.001	0.5094	0.0652	0.0009	0.7912	0.3633	0.2717

Table IV. Comparisons of element number and error $\left(J^{Ana.}-J\right)/J^{Ana.}(\%)$ between uniform mesh and non-uniform mesh for interface crack.

Mesh	Element number	Topological enrichment	Geometrical enrichment ($r_e=0.2a$)	Geometrical enrichment ($r_e=0.3a$)	Topological isotropic enrichment	Geometrical isotropic enrichment ($r_e=0.2a$)	Geometrical enrichment isotropic ($r_e=0.3a$)
$a/h_e=10$	200×400	0.6454	0.2015	0.1452	0.8880	0.4390	0.3492
$a/h_e^1=20$ $a/h_e^2=3$	94×154	0.4018	0.1389	0.1205	0.5311	0.2233	0.1923
$a/h_e^1=20$ $a/h_e^2=4$	112×192	0.3359	0.0689	0.0504	0.4615	0.1534	0.1223
$a/h_e^1=20$ $a/h_e^2=5$	130×230	0.3061	0.0362	0.0178	0.4290	0.1207	0.0897
$a/h_e^1=20$ $a/h_e^2=6$	148×268	0.2910	0.0184	0.0005	0.4113	0.1030	0.0719

Table V. Convergency study of the *J*-integral in terms of error $\left(J^{Ana.}-J\right)/J^{Ana.}(\%)$ with respect to the height of piezoelectric layers ($h_e^1=a/20$, $h_e^2=a/4$).

$2h/a$	Topological enrichment	Geometrical enrichment ($r_e=0.2a$)	Geometrical enrichment ($r_e=0.3a$)	Topological isotropic enrichment	Geometrical isotropic enrichment ($r_e=0.2a$)	Geometrical isotropic enrichment ($r_e=0.3a$)
10	0.3135	0.0227	-0.0016	0.4689	0.1214	0.0789
12	0.3845	0.1048	0.0814	0.5337	0.1998	0.1590
14	0.3122	0.0391	0.0163	0.5061	0.1804	0.1406
16	0.3399	0.0713	0.0494	0.4829	0.1595	0.1250
18	0.3610	0.0955	0.0744	0.5022	0.1814	0.1490